ANL/CMT/CP-96766

OXIDATIVE CORROSION OF SPENT UO_2 FUEL IN VAPOR AND DRIPPING GROUNDWATER AT 90°C*

RECEIVED
SEP 28 1999
OSTI

Robert J. Finch, Edgar C. Buck, Patricia A. Finn, and John K. Bates

Chemical Technology Division, Argonne National Laboratory
9700 South Cass Avenue, Argonne, IL 60439

Submitted for publication in the
Proceedings of the Materials Research Society
1998 Fall Meeting, Boston, Massachusetts,
November 30 – December 4, 1998

15 April, 1999

FINAL

* This task was performed under the guidance of the Yucca Mountain Site Characterization Project (YMP) and is part of activity D-20-43 in the YMP/Lawrence Livermore National Laboratory Spent Fuel Scientific Investigation Plan. This work was supported by the U.S. Department of Energy, under contract W-31-109-ENG-38.

DISCLAIMER

DISCLAIMER

OXIDATIVE CORROSION OF SPENT UO_2 FUEL IN VAPOR AND DRIPPING GROUNDWATER AT 90°C

ROBERT J. FINCH, EDGAR C. BUCK, PATRICIA A. FINN, and JOHN K. BATES
Argonne National Laboratory, 9700 South Cass Avenue, Argonne, Illinois 60439

ABSTRACT

Corrosion of spent UO_2 fuel has been studied in experiments conducted for nearly six years. Oxidative dissolution in vapor and dripping groundwater at 90°C occurs via general corrosion at fuel-fragment surfaces. Dissolution along fuel-grain boundaries is also evident in samples contacted by the largest volumes of groundwater, and corroded grain boundaries extend at least 20 or 30 grains deep (> 200 µm), possibly throughout millimeter-sized fragments. Apparent dissolution of fuel along defects that intersect grain boundaries has created dissolution pits that are 50 to 200 nm in diameter. Dissolution pits penetrate 1–2 µm into each grain, producing a "worm-like" texture along fuel-grain boundaries. Sub-micrometer-sized fuel shards are common between fuel grains and may contribute to the reactive surface area of fuel exposed to groundwater. Outer surfaces of reacted fuel fragments develop a fine-grained layer of corrosion products adjacent to the fuel (5–15 µm thick). A more coarsely crystalline layer of corrosion products commonly covers the fine-grained layer, the thickness of which varies considerably among samples (from less than 5 µm to greater than 40 µm). The thickest and most porous corrosion layers develop on fuel fragments exposed to the largest volumes of groundwater. Corrosion-layer compositions depend strongly on water flux, with uranyl oxy-hydroxides predominating in vapor experiments, and alkali and alkaline earth uranyl silicates predominating in high drip-rate experiments. Low drip-rate experiments exhibit a complex assemblage of corrosion products, including phases identified in vapor and high drip-rate experiments.

INTRODUCTION

Drip experiments have been used to investigate the corrosion of spent UO_2 fuel in a humid, oxidizing environment. Spent UO_2 fuels may be exposed to such an environment in the proposed repository at Yucca Mountain, Nevada [1,2]. Drip experiments with spent fuel use simulated groundwater that is periodically injected onto fuel fragments in stainless-steel reaction vessels kept at 90°C. Fuel reacts with the groundwater and with water condensed on fragment surfaces, precipitating a suite of corrosion products [2]. Two injection (drip) rates are employed: low drip-rate (LDR) experiments receive, nominally, 0.15 mL of simulated groundwater every week; high drip-rate (HDR) experiments receive approximately ten times that amount. Excess groundwater in all reaction vessels ensures that experiments are maintained at 100% relative humidity (RH). The simulated groundwater is J-13 well water that has been reacted with crushed Topopah Springs Tuff at 90°C for 80 days. The resulting solution, EJ-13 water, is higher in Na, K, and Si, and lower in Mg and Ca, than J-13 water [2,3]. In addition to drip experiments, vapor-hydration experiments are conducted at 90°C and 100% RH. No additional groundwater is injected in vapor experiments. Two pressurized-water-reactor fuels are used, ATM103 and ATM106 (rod NBD-107), which have burnups of ~30 MWd/kg-U and ~45 MWd/kg-U, respectively [4,5]. We are conducting six long-term corrosion experiments that have been running for nearly six years. A detailed understanding of corrosion products and processes identified in these experiments enhances our understanding of the potential behavior of spent nuclear fuel exposed to comparable conditions in a geologic repository.

ANALYTICAL METHODS

Experiments are periodically interrupted, vessels opened, and samples extracted for a variety of analyses. Solids are removed from surfaces of reacted fuel fragments by pressing fragments against double-stick cellophane tape in a petri dish within the hot cell. Extracted solids are examined by optical microscopy, and selected particles are isolated and either mounted onto conductive C-tape for analysis by scanning electron microscopy (SEM) or embedded in an epoxy resin. Embedded particles up to ~300 µm across are polished and examined by SEM; smaller particles (~5–30 µm) are ultramicrotomed and examined by transmission electron microscopy (TEM). Chemical analyses of solids are performed by energy dispersive spectroscopy (EDS), and selected TEM specimens are further analyzed by electron energy-loss spectroscopy (EELS). If sufficient material is available, samples are analyzed by X-ray powder diffraction (XRD).

RESULTS

After approximately five years, the surfaces of all fuel fragments in both drip and vapor experiments have developed yellowish to white crusts, obscuring the underlying (black) fuel. Analyses by SEM reveal these crusts to be predominantly U-bearing phases, including uranyl oxy-hydroxides and uranyl silicates (Table I). Similar phases were identified during corrosion studies of unirradiated UO_2 [1,3] and occur at many oxidized uraninite deposits in nature [6,7]. One novel uranyl phase has also been identified, $Cs_{2x}Ba_{1-x}(UO_2)_5MoO_6(OH)_6(H_2O)_n$ [8].

When experiments were started, fuel fragments were well indurated; however, during the 3.7-year sampling of one experiment (ATM103 HDR), a reacted fuel fragment crumbled while being manipulated. Scanning electron microscopic examinations of numerous particles from this fragment reveal gaps between grain boundaries (Fig. 1a), as well as curvilinear voids that give rise to a worm-like texture adjacent to fuel-grain boundaries (Fig. 1b). Similar features are not evident in polished sections of reacted fuel from LDR and vapor experiments; however, grain-boundary dissolution and a "wormy" texture were observed in fuel specimens exposed to Na-bicarbonate water in flow-through dissolution experiments [9]. Fuel-grain boundaries within fuel particles extracted from LDR and vapor experiments appear relatively unreacted, with few or no gaps between grains (Figs. 1c,d); however, only a few fuel-containing particles from LDR and vapor experiments have been examined by SEM.

Outer surfaces of fuel fragments from vapor and LDR experiments display a relatively dense, fine-grained layer of corrosion products adjacent to the fuel. The appearance and thickness of these corrosion layers vary among specimens, but they are approximately 5–15 µm thick (Fig. 1). A less dense, more coarsely crystalline outer layer of corrosion products covers the inner layers on most samples from vapor and LDR experiments. The thicknesses of the outer layers range from less than 5 µm to approximately 10 µm. Two morphologically distinct corrosion layers are evident on samples from the HDR experiments; however, both are more porous than corrosion layers formed in vapor and LDR experiments (Fig. 1). Corrosion layers on samples from HDR experiments are substantially thicker than corrosion layers formed on samples from LDR and vapor experiments, commonly exhibiting thicknesses in excess of 40 µm (Fig. 1). More recent optical examinations of reacted fuel fragments from HDR experiments indicate that corrosion layers continue to thicken over time, achieving thicknesses exceeding approximately 100 µm after nearly six years. Corrosion layers tend to thin to approximately 2–5 µm near corners of particles (Fig. 1c; *cf.* ref. [2]), suggesting that corrosion layers are expanded relative to the volume of fuel that was dissolved.

Scanning electron microscopy of corrosion products from HDR experiments reveals abundant acicular crystals of Na-uranyl silicate, which constitute most of the corrosion layer; minor Ca-uranyl silicate is detected most commonly along the outer regions of the corrosion layer (Table I). X-ray diffraction data indicate that the Na-uranyl silicate is Na-boltwoodite, $(Na,K)(UO_2)(SiO_3OH)(H_2O)_{1.5}$, and constitutes approximately 80 vol.% of the corrosion layer in HDR experiments. The Ca-uranyl silicate is β-uranophane, $Ca(UO_2)_2(SiO_3OH)_2(H_2O)_5$, which accounts for 20 vol.% or less of the corrosion layer in the HDR experiment on ATM103; it has not been confirmed in samples from experiments on ATM106. β-uranophane is most commonly observed in samples examined by TEM and is less commonly observed by SEM. This is because we obtain most TEM samples from the outermost part of corrosion layers, where β-uranophane seems most common.

Due to limited material, we have not conducted XRD analyses of corrosion products from LDR or vapor experiments and must base phase identifications on SEM and TEM analyses. Corrosion products from vapor experiments include metaschoepite, $(UO_2)_4O(OH)_6(H_2O)_5$ [10], and dehydrated schoepite, $(UO_2)O_{0.25-x}(OH)_{1.5+2x}$ $(0 \leq x \leq 0.15)$ [10,11], as well as minor $Cs_{2x}Ba_{1-x}(UO_2)_5MoO_6(OH)_6(H_2O)_n$ [8] (Table I). Common corrosion products from LDR experiments include metaschoepite; an unidentified Na-uranyl oxy-hydroxide tentatively identified as "Na-compreignacite," $(Na,K)_2[(UO_2)_3O_2(OH)_3]_2(H_2O)_7$; and soddyite, $(UO_2)_2SiO_4(H_2O)_2$. A few isolated crystals of Na-boltwoodite were first detected from the LDR experiment on ATM103 after 4.1 years; however, Na-boltwoodite is relatively abundant in

TABLE I. Uranium Corrosion Products from Spent UO_2 Fuel Reacted in Groundwater and Vapor.

PHASE	FORMULA	EXPERIMENT[1]		INTERVAL[2] (yr)
Metaschoepite	$UO_3{\cdot}2H_2O$	LDR: Vapor:	103 & 106 103 & 106	4.1 4.1
Dehydrated schoepite	$(UO_2)O_{0.25-x}(OH)_{1.5+2x}$ $(0 \leq x \leq 0.15)$	HDR: LDR: Vapor:	106 103 103 & 106	0.8 4.1 (?) 4.1
Na-UOH[3]	$(Na,K)_2[(UO_2)_3O_2(OH)_3]_2(H_2O)_7$	LDR:	103 & 106	4.1, 5.2
Soddyite	$(UO_2)_2SiO_4(H_2O)_2$	LDR:	103 & 106	4.1, 5.2
β-uranophane	$Ca(UO_2)_2(SiO_3OH)_2(H_2O)_5$	HDR:	103 & 106	3.7, 5.2(?)
Na-boltwoodite	$(Na,K)(UO_2)(SiO_3OH)(H_2O)_{1.5}$	LDR: HDR:	103 103 & 106	4.1, 5.2 3.7, 5.2
Cs-Ba-Mo-uranate	$(Cs,Ba)(UO_2)_5(MoO_6)(OH)_6(H_2O)_n$	HDR: LDR: Vapor:	106 103 106 & 103	0.8 4.1 4.1
Zr-U oxide	uncertain	LDR:	103	5.2
Zr-U-Pu oxide	uncertain (also Am, Ru & lanthanides)	HDR:	103	4.1

[1] 103 = ATM103 PWR fuel; 106 = ATM106 PWR fuel; LDR = low drip-rate experiment; HDR = high drip-rate experiment. [2] INTERVAL refers to sampling interval and indicates the total reaction time. [3] Possibly the Na analogue of compreignacite, $K_2[(UO_2)_3O_2(OH)_3]_2(H_2O)_7$.
(?) tentative phase identification for the interval indicated.

samples from the 5.2-yr sampling interval (ATM103). During SEM analyses of samples from the 5.2-yr reaction interval, we found several golden-brown spherules of an unidentified U-Zr oxide. A Pu-bearing U-Zr oxide was detected during TEM analyses of samples from the 4.9-yr sampling interval of the HDR experiment on AMT103.

DISCUSSION

The UO_2-fuel matrix of both fuels (ATM103 and ATM106) reacts in a similar fashion under all experimental conditions; however, the extent of reaction and the suite of U^{6+} corrosion products depend on the volume of water contacting the fuel and the reaction time.

Matrix dissolution

The spent-fuel matrix dissolves by three modes: (1) dissolution through the outer surface of fuel fragments (general corrosion) (Fig. 1); (2) dissolution along grain boundaries and defects associated with grain boundaries (Figs. 1a,b); and (3) dissolution of micrometer-sized intergranular fuel particles (Fig. 1b). The first mode is evident in samples from all three types of experiment (vapor, low drip rate, and high drip rate), whereas the second and third seem less significant for LDR and vapor experiments.

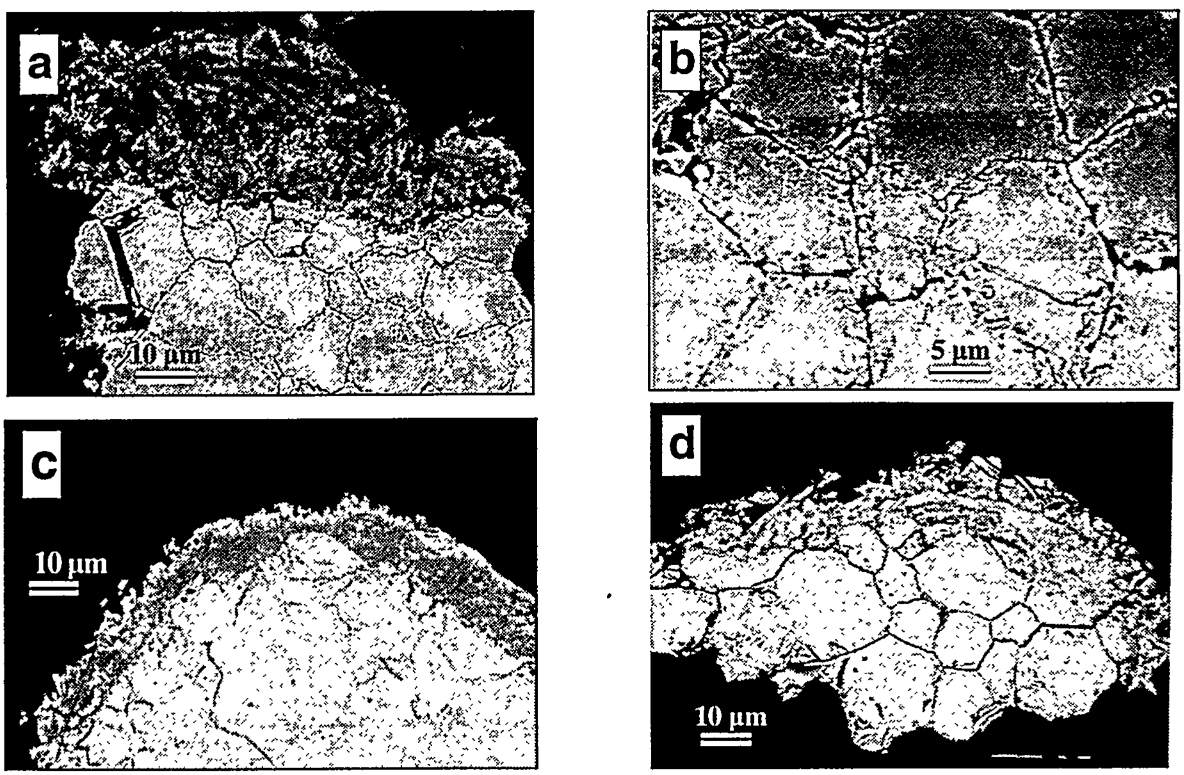

FIGURE 1. **(a)** Backscattered-electron image of a polished section through a fuel particle (bright contrast) from an HDR experiment with a corrosion layer (intermediate contrast) predominantly composed of Na-boltwoodite (ATM103 HDR 3.7 yr). **(b)** BSE image of a polished section showing curvilinear features at fuel-grain boundaries, which may result from dissolution along defects. Note fragmentation of grains along boundaries (ATM103 HDR 3.7 yr). **(c)** BSE image of a polished section and corrosion layer formed in an LDR experiment (ATM103 LDR 4.1 yr). **(d)** BSE image of a polished section with a corrosion layer of uranyl oxy-hydroxides formed in a vapor experiment (ATM103 Vapor 4.1 yr). Darkest contrast (black) in all images is epoxy.

Dissolution of fuel fragments in samples from all three types of experiment has proceeded through the outermost grains, with little or no preferential dissolution along adjacent grain boundaries (general dissolution). There is a distinct interface between inner and outer layers in samples from HDR experiments but no detectable difference in composition at the SEM scale. The physical significance of this interface is uncertain. We suspect that it represents the original outer surface of the fuel, although the degree to which the interface may have been displaced from its original position is uncertain. Some displacement might be expected because of the large volume difference between the original fuel and U(VI) corrosion products. Narrowing of layers near the corners of some fragments suggests expansion (Fig. 1c).

Dissolution along fuel-grain boundaries (mode 2) is observed in samples contacted by the largest volumes of dripping groundwater (HDR experiments) (Fig. 1b). Dissolution along grain boundaries extends at least 20 or 30 grains deep (> 200 μm) and possibly throughout entire fragments from HDR experiments. There seems much less dissolution along grain boundaries in samples from LDR and vapor experiments, where gaps between grains penetrate only a few grains deep (~10–30 μm). Dissolution of defects near grain boundaries appears minimal for fuel reacted in LDR and vapor experiments; however, specimens from low-drip and vapor experiments with fuel grains were difficult to obtain, and our observations are limited.

The "worm-like" texture observed near fuel-grain boundaries in samples from HDR experiments may be caused by preferential dissolution along defects (Fig. 1b). These curvilinear features penetrate 1 to 2 μm into each grain and may be responsible for fragmentation observed between fuel grains, especially in samples from HDR experiments. We have observed micrometer- to sub-micrometer-sized fuel particles in all polished samples. These small particles commonly occur between the larger fuel grains, although some fuel grains appear to have fragmented entirely into smaller pieces. The smallest particles are most abundant along grain boundaries in the HDR samples, where dissolution along defects may weaken the outer 1–2 μm of the grains. Weakening of grain-to-grain contacts, caused by dissolution along defects, may also explain the disaggregation of one large fuel fragment during the 3.7-year sampling [2]. These sub-micrometer-sized fuel particles may help to increase pathways available for infiltration of water to fragment interiors and can dramatically increase the reactive surface area of fuel samples.

<u>Corrosion products</u>

The suite of corrosion products identified from each experiment differs according to the composition and amount of water contacting fuel fragments (Table I; Fig. 2). Samples from vapor experiments display a relatively simple alteration-phase assemblage dominated by dehydrated schoepite and metaschoepite. This simple phase assemblage is readily explained by the lack of groundwater cations in vapor contacting the fuel surface. The only cations (except H^+) available for the precipitation of solids come from the dissolution of fuel. This effectively limits major alteration phases to simple uranyl oxy-hydroxides, such as metaschoepite and dehydrated schoepite. The Cs-Ba-Mo-uranate, first identified from a drip experiment [8], constitutes a common, although minor phase in vapor experiments. Both Cs and Mo are fission products, with Mo coming from corrosion of epsilon-Ru, or five-metal particles. The Cs-Ba-Mo-uranate may limit Cs and Mo early releases, especially in drip experiments; however, recent solution analyses indicate increasing Mo and Cs releases in HDR experiments, suggesting that this phase is transient.

Samples from LDR experiments possess a much more complex assemblage of U^{6+} phases than observed in either vapor or HDR samples. This complexity reflects the influx of EJ-13 groundwater, which contributes Si, Na, Ca, and other cations. The Cs-Ba-Mo-uranate has also been identified as a minor constituent in samples from LDR experiments, where it commonly occurs adjacent to dissolving fuel grains. We have limited direct evidence for the replacement of uranyl oxy-hydroxides by uranyl silicates: soddyite appears to replace Na-compreignacite in one sample from the 5.2-yr sampling of ATM103. Based on studies of UO_2 corrosion under similar conditions [1], this may become increasingly important at longer reaction times. In fact, the amount of Na-boltwoodite has increased substantially since it was first detected as isolated crystals in a sample from the 3.7-yr sampling interval. Nevertheless, Na-boltwoodite still seems to be less abundant than soddyite in LDR experiments. The unidentified U-Zr oxide is a minor phase (Table I), and we are uncertain at this time whether it is a corrosion product or occurs in the unreacted fuel.

Samples from HDR experiments display a relatively simple alteration-phase assemblage dominated by the two structurally related uranyl silicates, Na-boltwoodite and β-uranophane. The sequence of alteration-phase formation and replacement may be accelerated in HDR experiments compared with LDR experiments, so that this simple phase assemblage reflects relatively late-stage alteration (Fig. 2). The predominance of uranyl silicates in samples from HDR experiments may reflect replacement of earlier-formed uranyl oxy-hydroxides. Although we have not confirmed this in our experiments on fuel, it would agree with results of long-term drip experiments on unirradiated UO_2 [1,3] and with observations from naturally weathered uraninite deposits [6,7].

The formation and subsequent alteration of corrosion products may have a profound impact on the fates of certain radionuclides. Long-lived radionuclides that may affect the long-term safety of a geological repository include ^{237}Np, ^{99}Tc, ^{129}I, and ^{135}Cs. Barium and Sr are major substituents in β-uranophane, where they likely replace Ca in interlayer sites. Ruthenium and, to a lesser degree, Tc have also been detected as trace components of β-uranophane by TEM. These

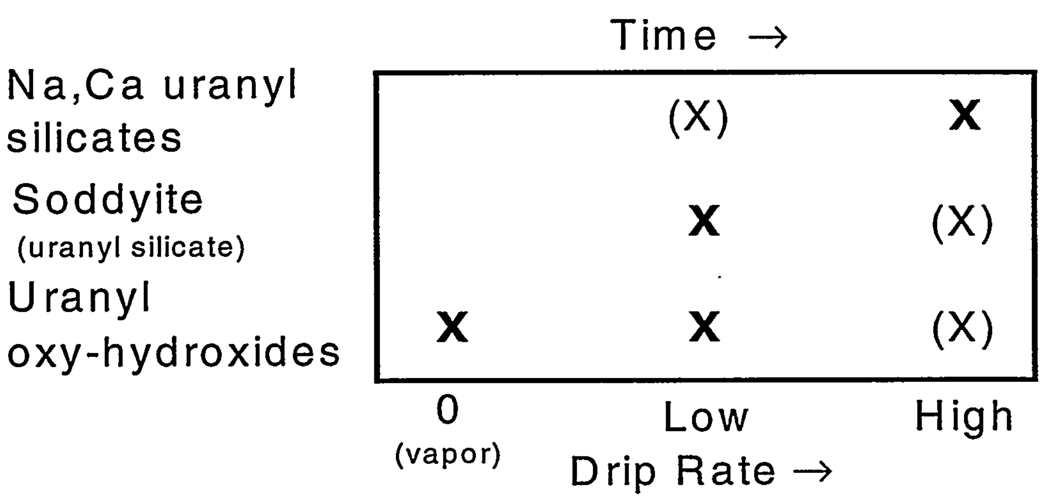

FIGURE 2: Schematic representation of alteration-phase paragenesis in unsaturated experiments with spent fuel. Bold Xs indicate major components of the alteration-phase assemblage; Xs in parentheses indicate minor components. Increased drip rates reproduce paragenetic relationships observed with increased time in experiments and in nature.

two elements may replace Si in very small amounts, but this has not been confirmed. Cesium has been detected in Na-boltwoodite. Recent ion-exchange experiments [12,13] suggest that Cs^+ may exchange with Na^+ and K^+ in Na-boltwoodite. The large surface area associated with corrosion layers (Fig. 1) makes Na-boltwoodite a potentially important sink for Cs in HDR experiments.

Neptunium-237 is a radionuclide of concern because of its potential mobility and long half-life (2.14 x 10^6 yr). Trace Np was detected in dehydrated schoepite extracted from vapor experiments, and electron energy loss spectra indicate that Np is incorporated into dehydrated schoepite in proportion to, or slightly in excess of, its concentration in unreacted fuel [14], which has a Np:U ratio of approximately 1:2000 [4]. Dehydrated schoepite may sequester a significant proportion of Np originally in the dissolved portion of the fuel. Although we have not yet identified Np-bearing solids in LDR or HDR experiments, lower-than-expected Np releases to solution may reflect Np incorporation into corrosion products in drip experiments as well.

The potential fate of Np in corrosion products

It is notable that we have identified Np in a uranyl oxy-hydroxide but not, as yet, in uranyl silicates. The NpO_2^+ ion should readily substitute for the uranyl ion (UO_2^{2+}) if local charge balance can be maintained [15]. The coupled substitution, $NpO_2^+ + OH^- = UO_2^{2+} + O^{2-}$, may maintain local charge balance in uranyl oxy-hydroxides, such as metaschoepite and dehydrated schoepite. This substitution mechanism for Np incorporation into dehydrated schoepite may operate in other uranyl oxy-hydroxides, including becquerelite, $Ca(UO_2)_6O_4(OH)_6(H_2O)_8$, and compreignacite, $K_2(UO_2)_6O_4(OH)_6(H_2O)_7$. However, this substitution may not be possible in uranyl silicates, such as soddyite, $(UO_2)_2SiO_4(H_2O)_2$, or uranophane-type structures, $M^{m+}[(UO_2)(SiO_3OH)]_m(H_2O)_n$, because O^{2-} ions in those phases bridge between Si^{4+} and U^{6+} ions. The only O atom not coordinated to a *Si* site in soddyite is a fully protonated H_2O group. As for uranophane-type silicates, only one O atom does not bridge between U^{6+} and Si^{4+}, and it is a protonated OH^- group coordinated to the Si atom. The lack of a charge-balancing mechanism for Np^{5+} substitution in uranyl silicates is consistent with our lack of evidence for Np in uranyl silicates examined so far.

Schoepite and similar uranyl oxy-hydroxides are transitory phases in the paragenesis of uraninite alteration in nature [6,7,16], as well as in experimental studies [1,3]; however, in some natural settings, schoepite can persist for many thousands of years [17]. The incorporation of Np into dehydrated schoepite may, therefore, be a long-term mechanism for Np retention from the standpoint of regulatory concern. The durability of dehydrated schoepite under conditions expected during the life of the repository at Yucca Mountain remains an important and poorly understood issue. Additional study is warranted, especially if Np is not incorporated into stable solids that may replace earlier-formed Np-bearing solids.

ACKNOWLEDGMENTS

This task was performed under the guidance of the Yucca Mountain Site Characterization Project (YMP) and is part of activity D-20-43 in the YMP/Lawrence Livermore National Laboratory Spent Fuel Scientific Investigation Plan. This work was supported by the U.S. Department of Energy under contract W-31-109-ENG-38. We are grateful to B. Tani and P. Johnson for help with XRD, and to J. Emery, L. Hoffenrichter, M. Clark, J. Falkenberg, and M. Surchik for technical support. T. DiSanto, N. Dietz, and J. Holly expertly prepared TEM samples. V. Oversby and an anonymous reviewer provided helpful comments on the manuscript.

REFERENCES

1. D.J. Wronkiewicz, J.K. Bates, S.F. Wolf, and E.C. Buck, J. Nucl. Mater. **238,** 78 (1996).
2. P.A. Finn, J.C. Hoh, S.F. Wolf, M.T. Surchik, E.C. Buck, and J.K Bates, in *Scientific Basis for Nuclear Waste Management XIX,* edited by W.J. Gray and I.R. Triay (Mater. Res. Soc. Symp. Proc. **465,** Pittsburgh, PA, 1997) pp. 527–534.
3. D.J. Wronkiewicz, J.K. Bates, T.J. Gerding, E. Veleckis, and B. Tani, J. Nucl. Mater. **190,** 107 (1992).
4. R.J. Guenther, D.E. Blahnik, T.K. Campbell, U.P. Jenquin, J.E. Mendel, and C.K. Thornhill, Pacific Northwest Laboratory Report PNL-5109-103 (1988).
5. R.J. Guenther, D.E. Blahnik, T.K. Campbell, U.P. Jenquin, J.E. Mendel, and C.K. Thornhill, Pacific Northwest Laboratory Report PNL-5109-106 (1988).
6. R.J. Finch and R.C. Ewing, J. Nucl. Mater. **190,** 133 (1992).
7. E.C. Pearcy, J.D. Prikryl, W.M. Murphy, and B.W. Leslie, Appl. Geochem. **9,** 713 (1994).
8. E.C. Buck, D.J. Wronkiewicz, P.A. Finn, and J.K. Bates, J. Nucl. Mater. **249,** 70 (1997).
9. W.J. Gray and C.N. Wilson, Battelle Pacific Northwest Laboratory Report PNL-10540 (1995).
10. R.J. Finch, F.C. Hawthorne, and R.C. Ewing, Can. Miner. **36,** 831 (1998).
11. R.J. Finch, F.C. Hawthorne, and R.C. Ewing, in *Scientific Basis for Nuclear Waste Management XIX*, edited by W.M. Murphy and D.A. Knecht (Mater. Res. Soc. Symp. Proc. **412**, Pittsburgh, PA, 1996) pp. 361–368.
12. P.C. Burns, J. Nucl Mater. **265,** 218 (1999).
13. R. Vochten, N. Blaton, O. Peeters, K. van Springel, and L. van Haverbeke, Can. Min. **35**, 735 (1998).
14. E.C. Buck, R.J. Finch, P.A. Finn, and J.K. Bates, in *Scientific Basis for Nuclear Waste Management XXI*, edited by I.G. McKinley and C. McCombie (Mater. Res. Soc. Symp. Proc. **506**, Pittsburgh, PA, 1998) pp. 87–94.
15. P.C. Burns, F.C. Hawthorne, and R.C. Ewing, J. Nucl. Mater. **245,** 1 (1996).
16. R.J. Finch, M.L. Miller, and R.C. Ewing, Radiochim. Acta **58/59,** 433 (1992).
17. R.J. Finch, J. Suski, K. Rasilainen, and R.C. Ewing, in *Scientific Basis for Nuclear Waste Management XIX*, edited by W.M. Murphy and D.A. Knecht (Mater. Res. Soc. Symp. Proc. **412**, Pittsburgh, PA, 1996) pp. 823–830.